Effectiveness of Multiple Pulses on Flow Index of Electroporation

Bashir I. Morshed*[a], Maitham Shams[b], Tofy Mussivand[c]
[a]Electrical and Computer Engineering, The University of Memphis, Memphis, TN, USA 38152;
[b]Dept. of Electronics, Carleton University, Ottawa, ON, Canada K1S 5B6;
[c]Medical Devices Innovation Institute, The University of Ottawa, Ottawa, ON, Canada K1Y 4W7

ABSTRACT

Electroporation is the formation of reversible pores in cell membranes without rupturing the membrane using a high electric field. Electroporation is an important technique for various biomedical applications including drug delivery, gene transfection and therapeutic treatments. A microfluidic device was developed to investigate electroporation using single and multiple pulses. The device contained integrated electrodes inside microchannels. Stained cells were introduced inside the microchannels and excitation pulses were applied. Sequences of images were captured using an integrated-camera on an optical microscope in the bright-field mode. Stained pixel data from the sequences of images were extracted through image processing to detect and quantify electroporation. Flow Index of EP (FIEP) was computed from the normalized (wrt initial) stained pixel data. Multiple pulses increased FIEP when increased energy was delivered, but reduced FIEP when the same amount of energy was delivered. Mean FIEP using 20 V excitation for 1 pulse of 1 ms was 0.256, 10 pulses of 1 ms was 0.329 and 1 pulse of 10 ms was 0.422. These experimental results show that a single pulse is more effective to induce higher FIEP compared to multiple pulses. FIEP enables quantitative and systematic study towards optimization of pulse parameters for electroporation-based applications.

Keywords: Drug delivery, electrical pulse, electroporation, Flow Index of electroporation, microchannel, microfluidics.

1. INTRODUCTION

When a cell is placed inside an electric field, charges accumulate along the cell membrane, inducing a potential across the membrane[1]. The induced membrane potential causes an electrical force on phospholipids, resulting in a stress for reorientation[2]. If the applied electric field is increased such that the induced membrane potential reaches a critical value, these phospholipids undergo conformal changes in membrane structure causing formation of a large number of hydrophilic pores (channels) through the cell membrane[3–5]. This phenomenon of a large number of reversible pore formation in the cell membrane due to a high electric field is known as electroporation (EP)[3-7]. EP causes a temporary loss of the semipermeability of cell membranes[8], resulting in ion leakage, escape of metabolites, selective release of intracellular molecules, increased uptake by cells of drugs, molecular probes, and genetic materials[9–13]. Medical applications of EP include intracellular or transdermal drug delivery, gene, ocular and vascular therapies[14, 15].

Extent of EP is dependent on a number of parameters including the electrical excitation durations, electric field magnitudes, number of excitation pulses, frequency, orientations of the electric field, cell size and shape, as well as buffer properties[16–20]. A major challenge of studying and comparing outcomes of EP experiments is the lack of systematic quantitative metric to allow comparative analysis and improved ability of classification. Previous studies have quantified EP outcomes through the percentage of cells undergoing EP detected by flow cytometry[21, 22] or fluorescence imaging[23–26], the amounts of stains uptake/cell measured through cell lysis using a calibrated microscope[27], the percentage of area coverage by stained cells after EP[28], delivery rates[29] and gene transfection rates[30]. An indirect approach utilized the increase in transmembrane conductance, as the conductance increases with higher extent of EP[16].

We have introduced a quantitative metric "Flow Index of electroporation" (FIEP) to quantify the extent of EP through a quantitative image analysis method with normalization[31]. FIEP is a numeric indicator of the severity of EP and relates to the probability of material/fluidic exchange between the cell and its environment through the cell membrane due to EP. Higher FIEP represents higher amounts of exchange. The minimum value of FIEP is 0 representing no occurrence of EP, and the maximum value is 1 representing complete loss of intracellular contents that occurs in the case of lysis. In this paper, we use this metric to quantitatively compare the effectiveness of multiple pulses compared to a single pulse.

*bmorshed@memphis.edu; phone 1 901 678-3650; fax 1 901 678-5469; esarp.memphis.edu

Nanosensors, Biosensors, and Info-Tech Sensors and Systems 2012, edited by Vijay K. Varadan,
Proc. of SPIE Vol. 8344, 834417 · © 2012 SPIE · CCC code: 0277-786X/12/$18 · doi: 10.1117/12.917435

Downloaded From: http://proceedings.spiedigitallibrary.org/ on 03/29/2013 Terms of Use: http://spiedl.org/terms

2. DEVICE, SETUP AND METHOD

Experiments were conducted with a microfluidic device fabricated through SensoNit Fabrication Process (Micronit Inc., Netharlads). The device consisted of two glass-slides (3 cm × 1.5 cm) thermally fused together. The top slide was 1.1 mm thick and contained conical-shaped access holes (ports). The bottom glass slide was 0.7 mm thick and chemically etched to form microchannels of 40 µm depth. A 200 nm thick metal electrode layer (180 nm Pt on top of 20 nm Ta) was deposited on the surface of the microchannel above the bottom slide before fusion. The microchannel, electrode layer and ports were designed using a layout editing CAD tool from MEMSPro v5.1 (SoftMEMS, CA, USA). An EP chamber was designed that housed 5 parallel microchannels of 12 mm long and 400 µm wide fluidically connected to two fluidic ports at both ends. Based on the layout features, the integrated electrode layer was named as Thick electrodes and Fingers. Fingers were 10 µm wide and 420 µm long strips of integrated electrodes that were laid at the bottom of each microchannel in perpendicular to the axis of the microchannel and used to generate electric fields inside the microchannels of the EP chamber. Alternative Fingers, spaced at 10 µm, were connected to two wide Thick electrodes on either side of a microchannel and forms an interdigitated configuration. Thick electrodes were electrically connected to external wires through two electrode ports and provided a low resistive path from Fingers to the external wires. Above the parallel microchannels, cell-loading ports were designed having the specification given in Figure 1(a-b). For fluidic connectivity, Nanoport assemblies (Upchurch Scientific, WA, USA) were affixed on top of the fluidic ports. For electrical connectivity, Silver Conductive Epoxy (Cat. 8331-14G, MG Chemicals, ON, Canada) was used inside the electrode ports to connect Thick electrodes with the external wires. A photograph of the post-processed device is shown in Figure 1(c).

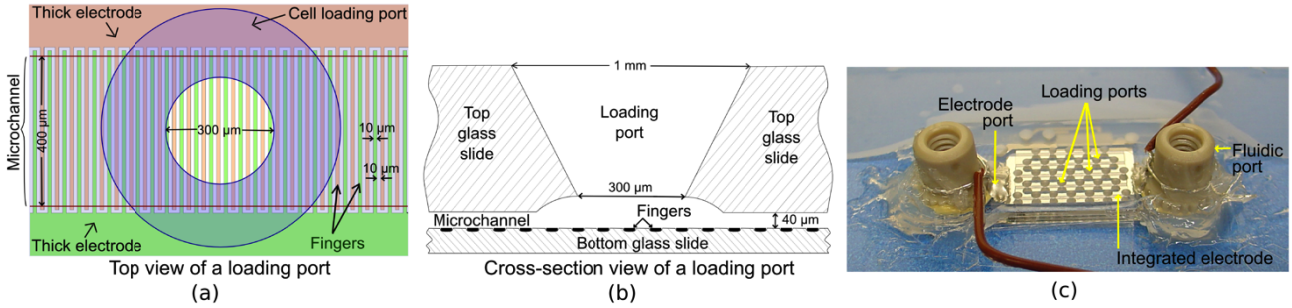

Figure 1. (a-b) A set of schematic drawings depicting the specification of a cell loading port, a microchannel and intedigitated electrode configuration of the integrated electrodes composed of Thick electrodes and Fingers. (c) A photograph of a fabricated microfluidic device (3 cm × 1.5 cm × 1.8 mm) after post-processing.

Human buccal cells were collected with sterilized swabs and stained with both Haematoxylin (Cat. 3530-16, Ricca Chemical, TX, USA) and Eosin Y (Cat. SE22-500D, Fisher Chemical, PA, USA) stains. Haematoxylin colors basophilic structures (such as chromosomes) with blue-purple hue, while Eosin Y colors eosinophilic structures (like cytoplasm) in bright pink or magenta. Cell nuclei were clearly visible in blue-purple hue inside the magenta colored cytoplasm. Average diameter of the sample cells was about 40 µm. The sample cells were stored in room temperature in a dark shelf, and no noticeable degradation of stains was observed even after 1 week of storage[31].

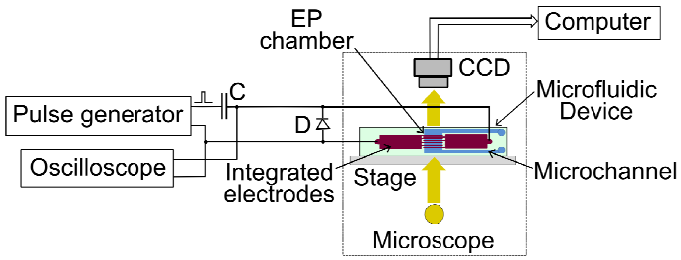

Figure 2. Schematic diagram of the experimental setup used for EP. The microfluidic device is electrically connected to a pulse generator and an oscilloscope through a capacitor (C) and a diode (D) and placed on top of the stage of an optical microscope equipped with a CCD camera that is connected to a computer workstation having an image capturing software.

Downloaded From: http://proceedings.spiedigitallibrary.org/ on 03/29/2013 Terms of Use: http://spiedl.org/terms

Prior to the initial use, the microfluidic device was wetted with 10% detergent solution (Triton X-100, Thermo Fisher Scientific, MA, USA) for 5 minutes and rinsed thoroughly with dd-H_2O. Prior to experimentation, the device was securely placed on top of the stage of an optical microscope (CKX41, Olympus Corp., IL, USA). The device was electrically connected with a signal generator (HP33120A, Hewlett-Packard Company, CA, USA) and an oscilloscope (TDS-3012, Tektronix Inc., OR, USA) with a capacitor, C, of 1 μF (SN010M050ST, Cornell Dubilier, SC, USA) and a diode, D, (IN4007, Texas Instruments, TX, USA) in revere bias configuration as shown in Figure 2. C and D would prevent accidental damage of the device from uncontrolled excitation, and eliminated DC offset voltages. The fluidic ports were connected to a pair of syringe pumps (Cat. 780100C, Cole-Parmer, IL, USA) through capillary tubing. Optical image sequences were captured in time-lapse mode (30 images at 5-seconds intervals) in bright-field mode with a 20× objective lens using a CCD digital camera installed in the trinocular port. The captured image sequences were ported with ImagePro Express software (Media Cybernetics Inc., MD, USA) and saved in raw AVI video format to the attached computer workstation.

The experimentation procedure was briefly as follows. A 10 μL of isotonic buffer fluid was injected inside the microchannels through the fluidic ports, and a 5 μL of the stained sample-cells were introduced inside the EP chamber through the cell loading ports. The microscope was then focused such that some of the stained cells are within the field of view of the microscope. The pulse excitation, the oscilloscope waveform recording, and the image capture sequence were initiated at the same instance using a synchronous external trigger. The excitation pulse magnitudes tested were 5 V, 10 V, 15 V and 20 V. The pulse-widths used were 10 μs, 100 μs, 1 ms, and 10 ms. Each pulse-train consisted of 1, 10, 25, or 100 pulses.

3. IMAGE ANALYSIS

The image-sequences captured from the CCD camera were analyzed using a Visual Basic (VB) script (Microsoft Corp., WA, USA) and a MATLAB code (The Mathworks Inc., MA, USA). Each image-sequence (video AVI file) contains 30 images captured at 5 s intervals starting from pulse excitation. A sample set of images from an EP experiment is shown in Figure 3. It is noted that electric pulses with higher magnitude and pulse widths produces bubbles due to hydrolysis of water, resulting in Brownian motion of cells. Reduction of Eosin Y stain was observed due to EP. This section describes the image processing methods used to quantify this reduction of stain.

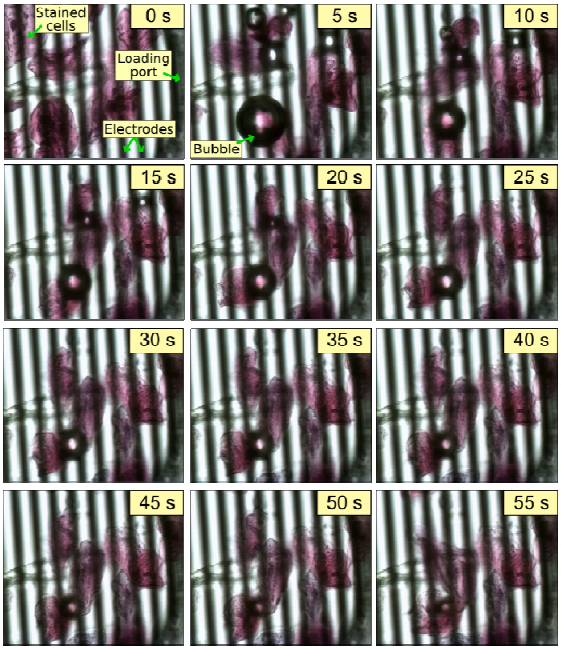

Figure 3. A set of images captured during an EP experiment that demonstrates a reduction of Eosin Y stain, formation of bubbles, as well as Brownian motion of cells. [Scale: Distance between the centers of adjacent vertical strips = 20 μm.]

Downloaded From: http://proceedings.spiedigitallibrary.org/ on 03/29/2013 Terms of Use: http://spiedl.org/terms

The pixel color range due to Eosin Y stain could be identified inside the region of interest (ROI) within the RGB color cube as shown in Figure 4. As the frames extracted from the raw AVI video are in 24-bit BMP (bitmap) format, the pixels within the ROI can be detected with proper threshold settings along R, G, and B values. The VB script performed this task and saved the number of stained pixels along each row and column, as well as the total number of stained pixels by analyzing each frame in a data file. The MATLAB code processed these data files to plot the number of stained pixels along the row numbers (y-axis plot) or column numbers (x-axis plot). Figure 5 shows a pair of frames of an image-sequence where the extracted stain data are plotted along the y-axis. The MATLAB code can also plot the total number of stained pixels from the data files of an image-sequence against the elapsed time after pulse excitation.

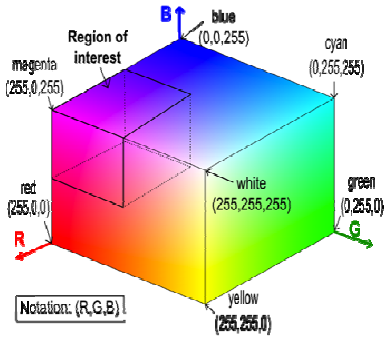

Figure 4. A RGB color cube drawn with MATLAB software showing red (R), green (G) and blue (B) axis. The 24-bit color scheme is denoted by the notation (R,G,B); where the values of R, G and B can be between 0 to 255. The region of interest (ROI) is indicated that represents the approximated range of colors for Eosin Y stain.

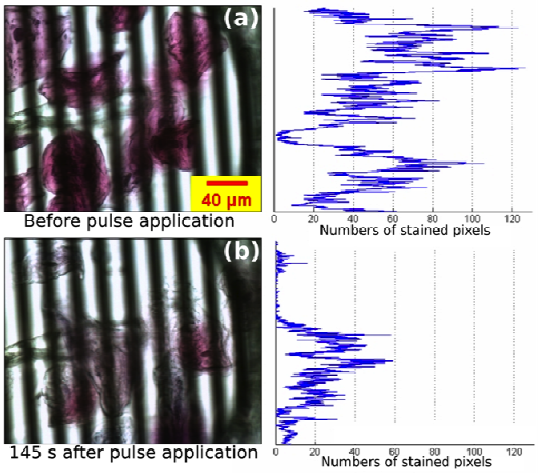

Figure 5. Plot of the extracted pixel data for a pair of frames from an image-sequence captured during an EP experiment. The extracted data plotted along the y-axis demonstrates a significant reduction of the number of stained pixels due to EP in the image taken 145 s after pulse excitation. [Scale: Distance between the centers of adjacent vertical strips = 20 µm.]

4. RESULTS

Experimental results demonstrated decreases of Eosin Y stain for various excitation pulse settings. Some cells have shrunken in diameters, indicating exodus of cytoplasmic fluids through the permeabilized membranes. Haematoxylin stain intensity remained unaltered and nucleus was clearly visible after experimentations, indicating that genetic materials have not exited the cells. The control cases, not excited by stimulus, did not show any sign of stain reduction.

To account for the random Brownian motion of cells, as well as to decorrelate the number of cells and the size of cells captured in in various experiments, the number of stained pixel data requires to be normalized. This parameter, denoted as "Normalized Stained Pixel" (NSP), can be expressed as follows,

Downloaded From: http://proceedings.spiedigitallibrary.org/ on 03/29/2013 Terms of Use: http://spiedl.org/terms

$$\text{NSP} = \frac{\textit{Number of stained pixels in a frame of the image}-\textit{sequence}}{\textit{Number of stained pixels in the first frame of that image}-\textit{sequence}}. \quad (1)$$

The temporal plot of the average NSP for EP experiments with a certain excitation criteria represents the rate of stain-loss of cells that diffuse in the surrounding environment. The plots from EP experiments have generally demonstrated exponential decay patterns from the initial state.

Figure 6, 7 and 8 demonstrate average responses of NSP for various excitation parameters. Control experiments without any electrical stimulation showed small fluctuations of average NSP, primarily due to Brownian motion of cells. The overall NSP change was less than 0.05 for all control cases. Figure 6, temporal plot of average NSP for various magnitudes of the applied voltages, suggests that increasing magnitudes of the pulses increase the rate of NSP reduction. Figure 7, where different numbers of pulses were applied, indicates that higher number of pulses results in higher amounts of NSP reduction.

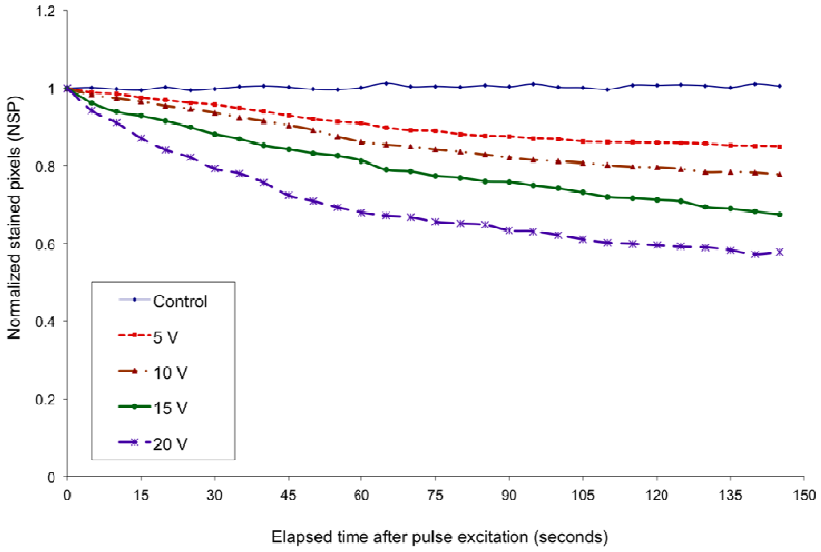

Figure 6. Temporal plot of average NSP (N=5) shows increase in reduction trend for a single pulse of increased magnitudes of the applied voltages, all having the same pulse width of 10 ms.

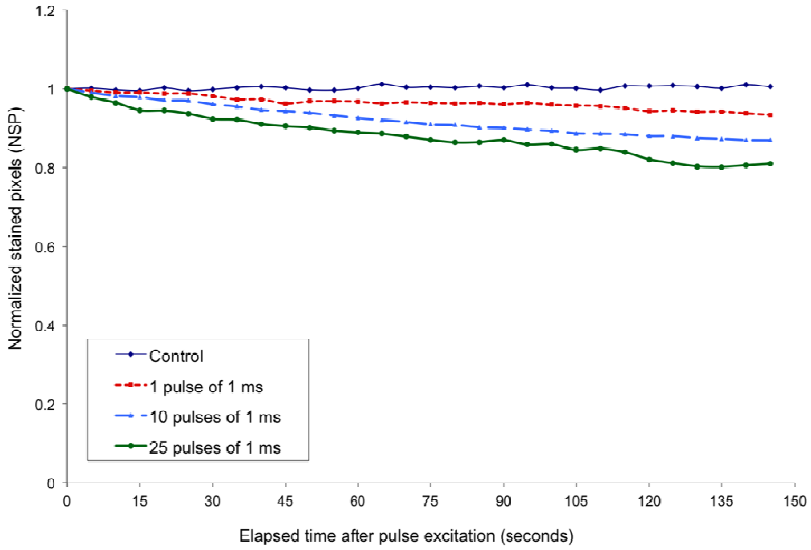

Figure 7. Temporal plot of average NSP (N=3) shows an increasing trend of reduction for increasing number of pulses, all having the same magnitude of 5 V and the same pulse-widths of 1 ms.

Downloaded From: http://proceedings.spiedigitallibrary.org/ on 03/29/2013 Terms of Use: http://spiedl.org/terms

Figure 8 presents temporal NSP plot of several cases of interest for applied voltage of 20 V. Comparing 1 pulse of 1 ms and 1 pulse of 10 ms, we find that longer pulse-widths produced larger reduction of NSP. The same can be deduced by comparing 10 pulses of 1 ms and 10 pulses of 10 ms. Meanwhile, the reductions of NSP for 100 pulses of 10 µs were less compared to the reduction due to 1 pulse of 1 ms, even though both contained the same amount of energy, as the energy content of a pulse-train can be given as,

$$\text{Energy content of a pulse-train} = \frac{(V)^2}{R} \times \sum_1^n T_i . \tag{2}$$

where V is the magnitude of the applied pulses, R is the path resistance, and T_i is the pulse width of i-th pulse in a pulse train of n-pulses. Similarly, the reductions of NSP for 10 pulses of 1 ms were less compared to that for 1 pulse of 10 ms, while both cases delivered the same amount of energy. These results suggest that a single pulse would case a higher amount of NSP reduction, thus a higher amount of fluidic/material would be exchanged through the permeabilized cell membranes, compared to multiple pulses.

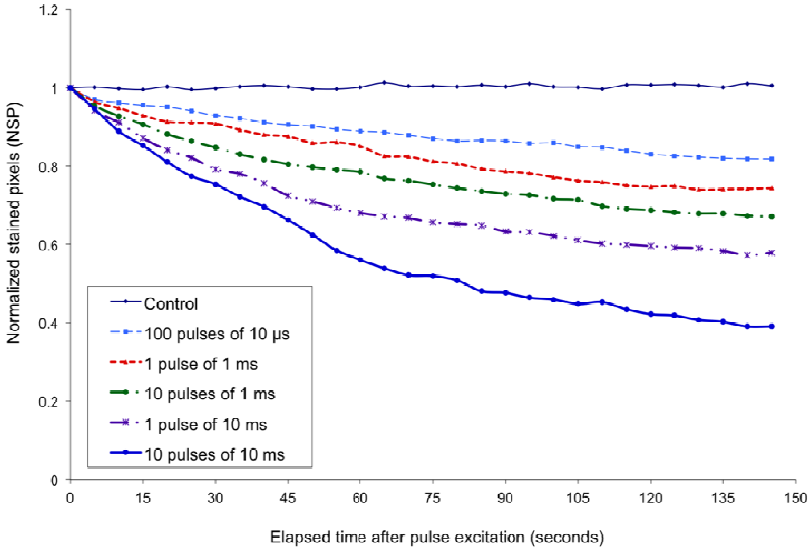

Figure 8. Temporal plot of average NSP (N=3) for various excitation parameters. In all of the cases, the pulse magnitudes were 20 V.

5. FIEP ANALYSIS AND DISCUSSION

As the spacing between adjacent Fingers is 10 µm, applied voltages of 5 V, 10 V, 15 V and 20 V would generate average electric fields of 5 kV/cm, 10 kV/cm, 15 kV/cm and 20 kV/cm, respectively, between Fingers. These electric fields were found to be sufficient to cause EP with various pulse-widths and number of pulses. For quantitative analysis, FIEP were calculated for each plot of average NSP. FIEP can be computed using the following relationship[31];

$$FIEP = 1 - Final\ value\ of\ the\ NSP \tag{3}$$

where "Final value of the NSP" would be ideally measured at the time, $t = \infty$. However, for practical measurements, a certain value of t needs to be assumed. In our experiments, the data from the last frame captured at 145 s has been considered as "Final value of the NSP". Since most experimental results showed indication of the NSP curves reaching asymptotic values, errors due to this approximation are expected to be insignificant.

FIEP values of five different sets of excitation conditions are presented in Figure 9. Each set consists of two excitation conditions that deliver the same amount of energy. In all of the cases, the excitation condition with higher number of pulses resulted in lower amount of FIEP. These results suggest that a single pulse causes the highest FIEP for certain amounts of energy, and thus is the most effective to induce higher extent of EP. For a particular level of energy delivery,

Downloaded From: http://proceedings.spiedigitallibrary.org/ on 03/29/2013 Terms of Use: http://spiedl.org/terms

FIEP resulting from a single pulse can be considered as the ceiling of achievable FIEP. As FIEP of 1 indicates complete lysis of cells, excitation conditions that would produce high levels of FIEP should be avoided for treatment of live cells.

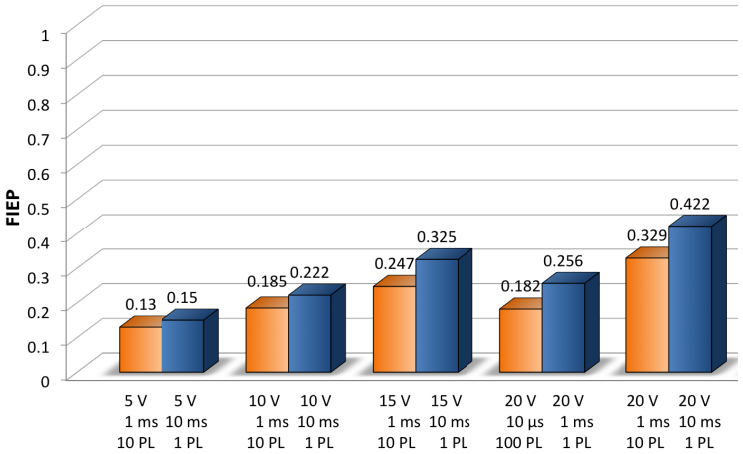

Figure 9. Plot of FIEP for five different sets of EP experimentation (N=3), where each set delivers the same amounts of energy with different number of pulses (PL).

6. CONCLUSION

This work demonstrated the utility of the metric FIEP to quantitatively determine and compare the effects of number of pulses in EP. The results indicated that increase amount of energy would produce higher amount of FIEP provided that other constrains are constant. However, multiple pulses produced less FIEP when compared to a single pulse delivering the same amount of energy. The quantification metric, FIEP, has allowed comparative study of different cases of EP and thus, is a useful metric that might aid in systematic analysis and optimization of EP-based applications including drug deliveries and various therapies.

REFERENCES

[1] Yao, C., Mo, D., Li, C., Sun, C. and Mi, Y., "Study of transmembrane potentials of inner and outer membranes induced by pulsed-electric field model and simulation," IEEE Trans. on Plasma Science, 35(5), 1541–1549 (2007).

[2] Hu, Q., Shidhara, V., Joshi, R. P., Kolb, J. F. and Schoenbach, K. H., "Molecular dynamics analysis of high electric pulse effects on bilayer membranes containing DPPC and DPPS," IEEE Trans. on Plasma Science, 34(4), 1405–1411 (2006).

[3] Joshi, R. P. and Schoenbach, K. H., "Electroporation dynamics in biological cells subjected to ultrafast electrical pulses: a numerical simulation study," Physical Review E, 62(1), 1025–1033 (2000).

[4] Tarek, M., "Membrane electroporation: a molecular dynamics simulation," Biophysical J., 88, 4045–4053 (2005).

[5] Moldovan, D., Pinisetty, D. and Devireddy, R. V., "Molecular dynamics simulation of pore growth in lipid bilayer membranes in the presence of edge-active agents," Applied Physics Letters, 91(20), 204104–3 (2007).

[6] Neumann, E., Sowers, A. E. and Jordan, C. A., [Electroporation and electrofusion in cell biology], Plenum Press, NY, USA (1989).

[7] Fox, M., Esveld, D., Valero, A., Luttge, R., Mastwijk, H., Bartels, P., van den Berg, A. and Boom, R., "Electroporation of cells in microfluidic devices: a review," Anal. Bioanal. Chem., 385, 474–485 (2006).

[8] Huang, Y. and Rubinsky, B., "Microfabricated electroporation chip for single cell membrane permeabilization," Sensors and Actuators, 89, 242–249 (2001).

[9] Fujimoto, H., Kato, K. and Iwata, H., "Electroporation microarrray for parallel transfer of small interfering RNA into mammalian cells," Anal. Bioanal. Chem., 392, 1309–1316 (2008).

Downloaded From: http://proceedings.spiedigitallibrary.org/ on 03/29/2013 Terms of Use: http://spiedl.org/terms

[10] Koda, S., Inoue, Y. and Iwata, H., "Gene transfection into adherent cells using electroporation on a dendrimer-modified gold electrode," Langmuir, 24(23), 13525–13531 (2008).
[11] Ionescu-Zanetti, C., Blatz, A. and Khine, M., "Electrophoresis-assisted single-cell electroporation for efficient intracellular delivery," Biomed. Microdevices, 10, 113–116 (2008).
[12] Wang, H. and Lu, C., "Microfluidic electroporation for delivery of small molecules and genes into cells using a common dc power supply," Biotechnology and Bioengineering, 100 (3), 580–586 (2008).
[13] Fei, Z., Wang, S., Xie, Y., Henslee, B., Koh, C. and Lee, L., "Gene transfection of mammalian cells using membrane sandwich electroporation," Anal. Chem., 79(15), 5719–5722 (2007).
[14] Dev, S. B., Rabussay, D. P., Widera, G. and Hofmann, G. A., "Medical applications of electroporation," IEEE Trans. on Plasma Science, 28(1), 206–223 (2000).
[15] Weaver, J. C., "Electroporation of cells and tissues," IEEE Trans. on Plasma Science, 28(1), 24–33 (2000).
[16] Maswiwat, K., Wachner, D. and Gimsa, J., "Effects of cell orientation and electric field frequency on the transmembrane potential induced in ellipsoidal cells," Bioelectrochemistry, 74, 130–141 (2008).
[17] Ibey, B. L., Mixon, D. G., Payne, J. A., Bowman, A., Sickendick, K., Wilmink, G. J., Roach, W. P. and Pakhomov, A. G., "Plasma membrane permeabilization by trains of ultrashort electric pulses," Bioelectrochemistry, 79(1), 114-121 (2010).
[18] Wang, H. and Lu, C., "High-throughput and real-time study of single cell electroporation using microfluidics: effects of medium osmolarity," Biotechnology and Bioengineering, 1116–1125 (2006).
[19] Ziv, R., Steinhardt, Y., Pelled, G., Gazit, D. and Rubinsky, B., "Microelectroporation of mesenchymal stem cells with alternating electrical current pulses," Biomed. Microdevices, 11, 95–101 (2009).
[20] Agarwal, A., Zudans, I., Weber, E. A., Olofsson, J., Orwar, O. and Weber, S. G., "Effect of cell size and shape on single-cell electroporation," Anal. Chem., 79(10), 3589–3596 (2007).
[21] Chen, C., Evans, J. A., Robinson, M. P., Smye, S. W. and O'Toole, P., "Measurement of the efficiency of cell membrane electroporation using pulsed ac fields," Phys. Med. Biol., 53, 4747–4757 (2008).
[22] Kima, J. A., Choa, K., Shin, M. S., Lee, W. G., Jung, N., Chunga, C. and Changa, J. K., "A novel electroporation method using a capillary and wire-type electrode," Biosensors and Bioelectronics, 23, 1353–1360 (2008).
[23] He, H., Chang, D. C. and Lee, Y., "Using a micro electroporation chip to determine the optimal physical parameters in the uptake of biomolecules in hela cells," Bioelectrochemistry, 70, 363–368 (2007).
[24] Wang, H. and Lu, C., "Electroporation of mammalian cells in a microfluidic channel with geometric variation," Anal. Chem., 78(14), 5158–5164 (2006).
[25] Wang, J., Stine, M. J. and Lu, C., "Microfluidic cell electroporation using a mechanical valve," Anal. Chem., 79(24), 9584–9587 (2007).
[26] Kim, S. K., Kim, J. H., Kim, K. P. and Chung, T. D., "Continuous low-voltage dc electroporation on a microfluidic chip with polyelectrolytic salt bridges," Anal. Chem., 79(20), 7761–7766 (2007).
[27] Kennedy, S. M., Ji, Z., Hedstrom, J. C., Booske, J. H. and Hagness, S. C., "Quantification of electroporative uptake kinetics and electric field heterogeneity effects in cells," Biophysical J., 94, 5018–5027 (2008).
[28] Olbrich, M., Rebollar, E., Heitza, J., Frischauf, I. and Romanin, C., "Electroporation chip for adherent cells on photochemically modified polymer surfaces," Applied Physics Letters, 92, 013901–3 (2008).
[29] Huang, K., Lin, Y., Su, K. and Chen, H., "An electroporation microchip system for the transfection of zebrafish embryos using quantum dots and GFP genes for evaluation," Biomed Microdevices, 9, 761–768 (2007).
[30] Kima, J. A., Choa, K., Shin, Y. S., Jung, N., Chunga, C. and Changa, J. K., "A multi-channel electroporation microchip for gene transfection in mammalian cells," Biosensors and Bioelectronics, 22, 3273–3277 (2007).
[31] Morshed, B. I., Shams, M., and Mussivand, T., "Identifying severity of electroporation through quantitative image analysis," Applied Physics Letters, 98, 143704–3 (2011).

Downloaded From: http://proceedings.spiedigitallibrary.org/ on 03/29/2013 Terms of Use: http://spiedl.org/terms